JOM, Vol. 67, No. 5, 2015
DOI: 10.1007/s11837-015-1381-0

Thermal Management in Friction-Stir Welding of Precipitation-Hardened Aluminum Alloys

PIYUSH UPADHYAY[1,3] and ANTHONY P. REYNOLDS[2]

1.—Pacific Northwest National Laboratory, Richland, WA 99354, USA. 2.—Department of Mechanical Engineering, University of South Carolina, Columbia, SC 29208, USA. 3.—e-mail: Piyush.Upadhyay@pnnl.gov

Process design and implementation in friction-stir welding (FSW) is mostly dependent on empirical information. Basic science of FSW and processing can only be complete when fundamental interrelationships between the process control parameters and response variables and the resulting weld microstructure and properties are established to a reasonable extent. It is known that primary process control parameters such as tool rotation, translation rates, and forge axis force have complicated and interactive relationships to process-response variables such as peak temperature and time at temperature. Of primary influence on the other process-response parameters are temperature and its gradient in the deformation and heat-affected zones. Through a review of pertinent works in the literature and results from boundary condition experiments performed in precipitation-hardening aluminum alloys, this article partially elucidates the nature and effects of temperature transients caused by variation of thermal boundaries in FSW.

BACKGROUND AND INTRODUCTION

Friction-stir welding (FSW) has evolved substantially since its invention in 1991. It has been implemented in industrial practice and has been widely investigated in research laboratories around the world. A large body of knowledge has thus accumulated over the years, leading to wider understanding of the process[1–3] Nevertheless, much needs to be done before the process can be optimized to obtain the desired postweld microstructure and properties for given service requirements, such as strength, ductility, and fatigue, without conducting a thorough process development for specific alloy and gauge combinations. The statement, "New welding technology is often commercialized before fundamental science emphasizing the underlying physics and chemistry can be developed,"[4] made prior to the advent of FSW, is applicable. Like most new inventions that are readily adopted by industries, "technological developments have far exceeded efforts in fundamental research [in FSW]."[5] Currently, process design and implementation are still mostly based on empirical information and anecdotal evidence. An improved understanding of cause-and-effect relationships between process control variables, including tool rotational and translation rates, tool geometry, tool material, and forge force, and response parameters such as stir zone and heat-affected zone (HAZ) temperature histories and the resulting joint properties, would facilitate wider acceptance and implementation of FSW. Of primary influence on the other process-response parameters is the nature of the temperature field in the deformation and heat-affected zones. The resulting weld properties and process responses, including tool torque and forces, are all affected by the temperature transients that the weld experiences. These temperature transients are directly affected by thermal conditions at different boundaries during the welding process as well as the direct action of the tool on the workpiece. Through an extensive review of pertinent literature and results from boundary condition experiments performed in precipitation-hardening aluminum alloys, this article partially elucidates the nature and effects of temperature transients caused by variation of thermal boundaries in FSW.

THERMAL MANAGEMENT IN FRICTION-STIR WELDING: OVERVIEW

A block diagram schematically illustrating the relevant heat flows during a typical friction-stir

(Published online March 25, 2015)

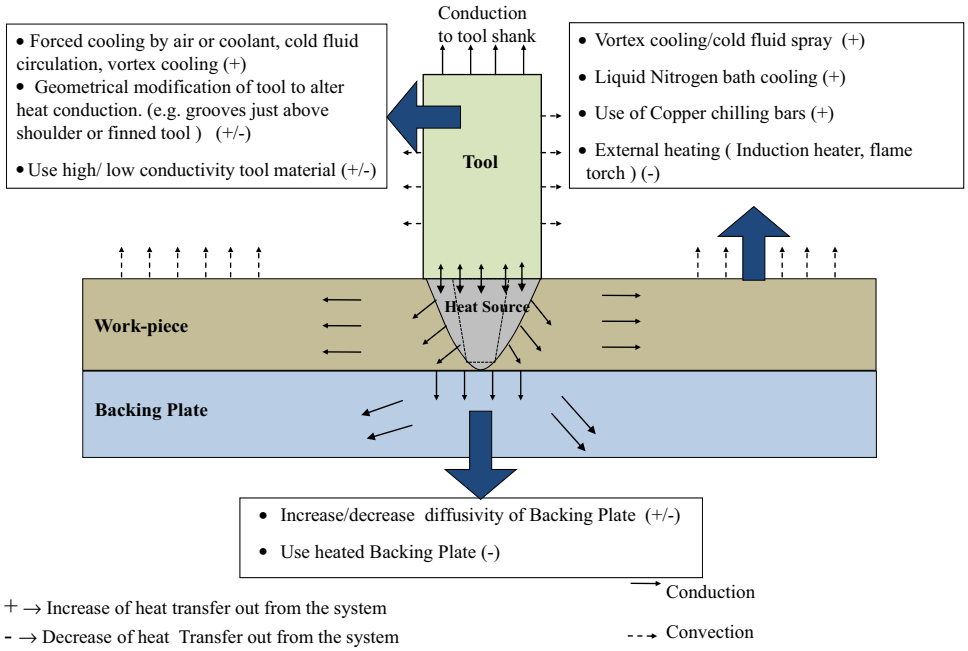

Fig. 1. Some representative thermal management methods that can be applied in friction stir welding. Arrows indicate the direction of heat transfer. The line type of the arrows indicates the dominant mode of heat transfer (solid: conduction; dotted: convection).

weld is shown in Fig. 1. Thermal management in FSW can be achieved by modifying thermal conditions at the different boundaries of the process zone including the tool, backing plate (BP), and the workpiece. A comprehensive list of thermal management techniques that could be applied to change thermal conditions at these boundaries is shown in Fig. 1. The "+" and "−" signs beside each method are indicative of whether the adopted method increases (+) or decreases (−) the heat-transfer rate from the FSW system, with everything else remaining constant. For example, the use of auxiliary cooling on the top of the workpiece enhances the heat transfer away from the weld zone, while active heating of the top surface or a heated BP retards transfer of heat away from the system. Additionally, the initial temperature of the workpiece may be adjusted to change lateral heat transfer from the weld zone.

Thermal management has long been used to achieve better post-weld properties and ease of joining. A patent from 1966, for example, discusses the use of liquid nitrogen and an acetone/dry-ice mixture to enhance the post-weld properties of stainless steel joints for high-pressure applications.[6] When administered appropriately, thermal management enables better control over the process response and can be used to obtain desired weld conditions and properties. In FSW, published works pertaining to modification of thermal boundaries are motivated toward achieving specific weld properties, such as enhanced mechanical properties, reduced residual stresses, or decreased corrosion susceptibility.

Rapid in-process quenching, for example, has been shown to result in ultrafine grain structure leading to room-temperature superplasticity of the weld nugget. Early work in in situ quenching can be attributed to Benavides et al.[7] wherein aluminum-alloy (AA) 2024 plates were friction-stir processed while submerged in liquid nitrogen, resulting in submicron-sized grains. Rhodes et al.[8] achieved recrystallized grains of 25–100 nm in AA7050 using a "plunge and extract" technique.

Rapid quenching has long been used to improve the properties of precipitation-hardened materials. Sakurada et al. used the inertia friction welding method to join cylindrical AA6061 components under water. Comparing the underwater welds with regular welds performed in air, they reported a 14% increase in joint efficiency (joint ultimate tensile strength [UTS] divided by base metal UTS) and decrease in the width of the HAZ. Nelson et al.[9] performed FSW by externally heating and cooling the parent metal plate and anvil. Cold water and mist were used to chill the plates in the wake of the tool. They reported a maximum 10% increase in tensile strength in FSW of AA7075-T7 after post-weld natural aging (PWNA). Su et al.[10] reported the production of nanosize grains and ultrafine grains in an AA7075 sheet by quenching the workpiece behind the tool with a mixture of water, methanol, and dry ice. Similar results were reported by Hofmann and Vecchio[11] for AA6061 by welding under water. Fratini et al.[12] performed welds with relatively thin (3 mm) AA7075 in regular forced air and underwater cases using three sets of welding parameters. Underwater welds were reported to

have slightly better strength in all the three welding conditions. Hosseini and Manesh[13] performed underwater welding of an accumulative roll-bonded aluminum alloy. Lower grain size, narrower HAZ, and slight increase in yield and tensile strength were reported. Bloodworth[14] reported a similar increase in tensile strength when welds were performed both in air and underwater. A 20% increase in the torque and hence power required for underwater welding was also reported. Fu et al.[15] also reported strength increases of up to 14% welding AA7050 underwater. Methods of tool cooling using liquids or forced air have also been used to control deformation-zone temperature. Such methods have been claimed to reduce the surface irregularity and increase the welding speed window as well.[16]

On the opposite end of thermal management, heating the work piece to retard the heat loss has also been used. Preheating of metals is known to provide for better machining performance. Preheating is especially useful for high-temperature alloys such as steel so that welding can be done at relatively high speeds with lower tool forces, thus enhancing tool life. A straightforward method to achieve this has been to attach a heat source directly in front of the tool so that the material immediately ahead of the tool is at an elevated temperature and thus is more easily plasticized during subsequent welding. Patents such as those in Refs. 17 and 18 make use of this technique using laser and tungsten-inert-gas arc as heat sources. Demonstrating the use of an yttrium-aluminum-garnet laser ahead of the tool during FSW of AZ91D Mg alloy, Kohn et al.[19] reported a reduction in tool forces. The use of induction preheating was shown to reduce *X*, *Y*, and *Z* forces and torque by 30%, 110%, 10%, and 20% respectively, in FSW of 6-mm-thick 1018 steel.[20] Sinclair et al.[21] investigated, in a fairly detailed manner, the effects of preheating the work piece on measured torque and forge force. Both position- and force-control schemes were used by varying the welding speeds. Most of the welds reported have volumetric worm-hole defects, suggesting less-than-ideal material flow. A reduction (as high as 43%) in the forge force with preheated plates was reported. Increased initial plate temperature produced a similar reduction, followed by a plateau, in the measured torque. Convergence of the measured torque for all the cases at the highest initial plate temperature is indicative of the self-limiting nature of heat generation during the process. Lotfi and Nourouzi[22] recently reported on welds made with 3-mm-thick AA7075 that employed preheating the weld seam just ahead of the FSW tool and softening of the material prior to welding, which resulted in defect-free welds even using unsuitable parameters. Nevertheless, the overall strength of joints reported was relatively low. A downside of bulk workpiece preheating has to be recognized here. With the reduction of natural quenching rate, the precipitation-hardenable alloys will suffer overaging postwelding, especially in the HAZ. This can be avoided by judicious use of heating and/or subsequent auxiliary cooling strategies. Other than managing the tool forces and increasing the welding speed window, the thermal situation at the workpiece is important in determining critical process-response parameters such as stir zone temperature, cooling rate, and torque. The amount of heat generated that is actually available for plastic deformation and recrystallization is dependent directly on the thermal situation at the bottom of the workpiece.

Rosales et al.[23] reported welds made with AA2024 and AA6013 in which steel, copper, and ceramic-coated BPs were used with three combinations of rotational and welding speeds while the forge force was kept constant.[23] Deformation-zone temperatures were not measured, whereas the in-plate far-field temperature measurements varied significantly when using different BPs. Weld cross-section macrographs indicate thinning of the cross-section, probably because of high flash content in welds made with the ceramic-coated BP. As part of a quench sensitivity study, Nelson et al.[9] reported that the use of a heated BP resulted in higher peak temperature and lower cooling rate, which produced inferior mechanical properties in AA7075 welds. Some researchers have used thermal management at the BP to optimize the friction-stir spot welding (FSSW) process in relatively thin sheets. Su et al.[24] for instance, reported that in FSSW of 1.3-mm-thick AA6111, a greater fraction (from 12.5% to 50%) of energy generated by the tool was transferred as heat energy into the weld zone when a mica clamp and BP were used in place of a conventional steel clamp and BP. This is reasonable since greater insulation reduces the heat dissipated into the BP. In a similar study, in FSW of 0.9-mm-thick AA6111, Bakavos et al. found that the use of a ceramic BP resulted in a 45°C increase in the peak processing temperature and a 15% reduction in lap shear strength compared with a conventional steel BP.[25]

EXPERIMENTAL PROCEDURE

The welds reported in this work were produced using a MTS FSW Process Development System (MTS Systems Corporation, Eden Prairie, MN) using the forge load-control method. A wide spectrum of weld runs was made in three materials: AA6056 (4.2 mm thick), AA7050 (6.35 mm thick), and AA6061 (25.4 mm thick), with systematic variation of boundary conditions at the workpiece surface and the BP. For the case of 6.35-mm-thick AA7050, welds were made with plates in room temperature air (IA) or completely submerged in water (UW) and with plates submerged in a mixture of 40% ethylene glycol and 40% water with 10% of dry ice (referred to as sub-ambient [SA]), resulting in a steady-state far-field temperature of −25°C. For the case of the 4.2-mm-thick AA6056 and 25.4-mm-thick AA6061,

the welds were made using four different types of BP with widely varying thermal diffusivity, viz. AA2099, tool steel, Ti-6-4, and ceramic flooring tile. The tools used for production of all the welds were of two-piece design with a single scroll, typically made out of H13 tool steel, and a probe fabricated out of MP-159 (a high-temperature cobalt-based superalloy) in the shape of a truncated cone (8° taper) with threads and three flats. For 6.35-mm-thick AA7050 welds, the shoulder was 17.8 mm in diameter and the probe was 6.1 mm long, with a diameter of 7.9 mm at the intersection with the shoulder. The same tool was used for 4.2-mm-thick AA6056 by adjusting the probe length to 4.1 mm. For 25.4-mm-thick AA6061, a 35-mm diameter shoulder was used with a 25.2-mm-long probe.

The temperature measurements in the plates were made by attaching thermocouple (TC) beads at approximate locations of HAZ minimum hardness, which typically occurs at about 5–10 mm from the weld seam, depending primarily on welding speed and alloy composition. The TCs were peened into the plate at chosen locations. Vickers hardness testing was used to assess the changes in the mechanical property of the joint after welding. Hardness was measured on a transverse cross-section at different thickness levels (primarily in the midplane). Testing was done on a Buehler Micromet 1 hardness testing machine (Buehler, Lake Bluff, IL) with a diamond-shaped indenter.

RESULTS AND DISCUSSIONS

Figure 2 shows a plot of peak temperatures and average tool torques versus the tool rotation rate for 6.35-mm-thick AA7050 welds made under ambient conditions (no auxiliary cooling, steel BP, laboratory air) and underwater. The peak temperatures were obtained from a TC attached inside the tool probe on the axis of rotation at the weld midplane. In this study, the welding speed was changed with the rotational speed such that an advance per revolution of 0.5–0.7 mm was maintained. Owing to enhanced heat transfer from the tool and plate into the surrounding water, the peak probe temperature is consistently lower for underwater welds than the corresponding in-air welds. The higher torque observed for underwater welds is related to lower temperature of the material in contact with the tool. Two important outcomes from this series of experiments are as follows: (1) The peak probe temperature is inversely correlated with the measured torque and (2) both those quantities approach limiting values that depend on the alloy in question as the rotation rate is increased. This limiting value is also determined by the thermal boundary condition applied at the surface of the workpiece. The higher the rotational speed, the higher will be the temperature causing the material flow stress to decrease. This decrease in flow stress in turn will limit the power generation by plastic dissipation and the temperature increase. A similar trend in peak temperature with varying rotational speed was reported by Sato et al.[26] for AA6063. This type of correlation can be valuable in weld process development for new combinations of alloy and thickness, and it can provide useful information while optimizing weld control parameters.

A concern with graphs like that in Fig. 2 not only the tool rotation rate is varied. When making a series of welds with varying tool rotation and/or welding speed, the FSW practitioner will invariably have to adjust the applied forge force or the tool position as well depending on control scheme to produce defect-free welds with minimal flash. Unfortunately, such parameters are rarely reported in the published works. Take force control for instance: For any given combination of tool rotation rate and welding speed, there will be an empirically established "optimum" forge force that provides adequate shoulder contact without causing excessive flash. If the rotation rate is increased or welding speed decreased without any forge force adjustments, then some of the plasticized material will be expelled from under the shoulder instead of being consolidated behind the tool, resulting in excessive flash and possibly volumetric defects. Conversely, if the rotation rate is decreased or welding speed is increased, then an increase in forge force is required to maintain sufficient shoulder contact with the plate and prevent defect.

Figure 3 illustrates how gradually changing the forge force while keeping all other parameters constant changes the weld quality. Welds were made with different forge forces in 4.2-mm-thick AA6056-T4 at 640 rpm and 6.8 mm/s. In this series, the BP material was also varied to observe the effects of changes in thermal condition at the bottom of the workpiece while keeping tool RPM and welding speed constant. Each column shows weld surfaces produced by welding on BPs made from a particular material. The thermal diffusivity of the BP materials increases from left to right (increasing heat loss

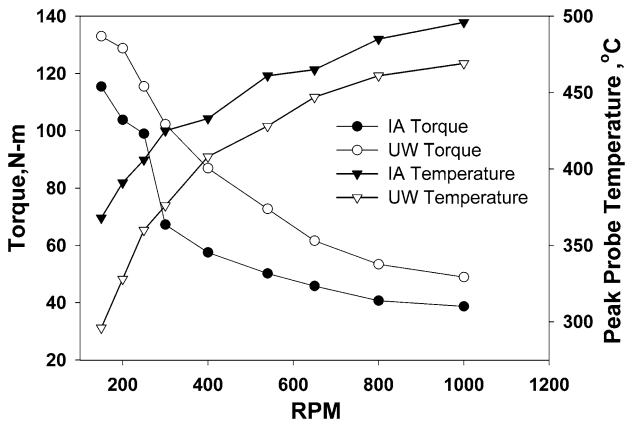

Fig. 2. Measured torque and peak temperature plotted against the tool rotation rate for welds made in air and underwater.[27]

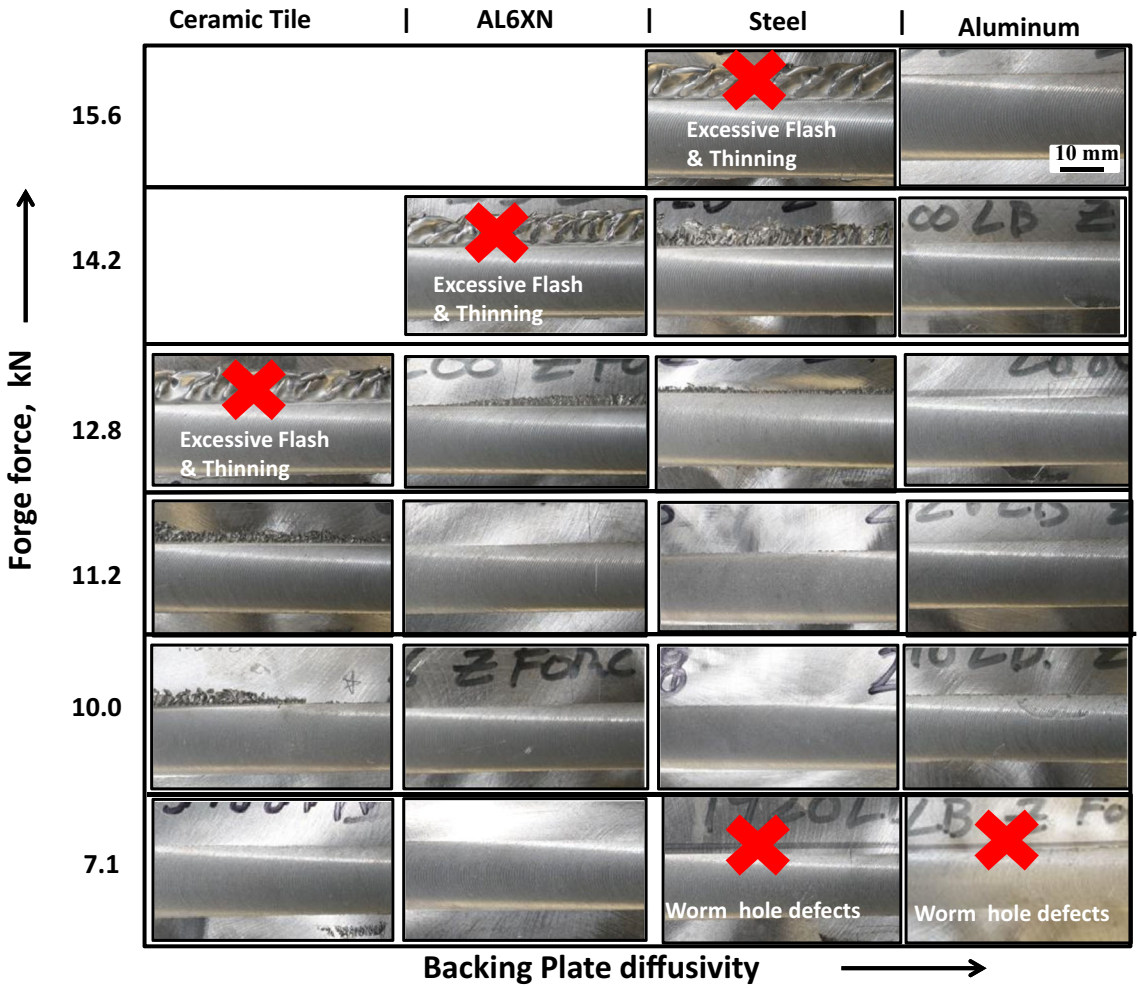

Fig. 3. Representative weld surfaces from series of welds made at 640 rpm and 6.8 mm/s in 4.2-mm-thick AA6056. Welds made with different BPs are shown in different columns, while each row shows welds made at the indicated forge force. The scale is shown on the top right corner applicable for all the individual images.

from the workpiece to the BP). Each row shows weld surfaces produced by welding using forge forces ranging from 7.1 kN to 15.6 kN, increasing from the bottom to the top in each column. For a given BP, starting with low forge force, there is incomplete shoulder contact to begin with, and as the forge force is increased (bottom to top), full shoulder contact is achieved. At the higher levels of forge force, excessive flash occurs. At a given forge force, the extent of shoulder contact and level of flash seem to be dependent on the heat loss to the bottom of the BP. For instance, whereas welds made with a ceramic BP at a forge force of 12.8 kN result in excessive flash, shoulder contact is just sufficient using an aluminum BP with everything else remaining constant, including the forge force. Consequently as heat transfer from the workpiece via the BP increases, the optimum forge force increases. Variation in BP material also resulted in a significant variation in peak temperature at the stir zone as reflected in the tool temperature as discussed next.

Considering defect-free welds with acceptable flash conditions, the combined variation of forge force and BP diffusivity resulted in as much as 70°C difference in measured peak temperature, viz. 390°C at 8.5 kN with an aluminum BP to 460°C at 11.3 kN with a ceramic BP (see Fig. 4). Additional information related to this work is available in Ref. 28. The results discussed above clearly show that the BP thermal properties have a significant effect on the peak temperature and consequently the weld properties. However, because the workpiece plate thickness used was relatively low, the through-thickness effect of BP thermal conditions cannot be fully examined. Thick plates (20 mm and above) can be difficult to friction-stir weld because uneven distribution of the heat source leads to either an overheated crown or underheated root. Because the root side is farther away from the shoulder heat source, greater power levels (achieved by increasing rotation rate or forge force or both) are needed to ensure desired material mixing in the root region.

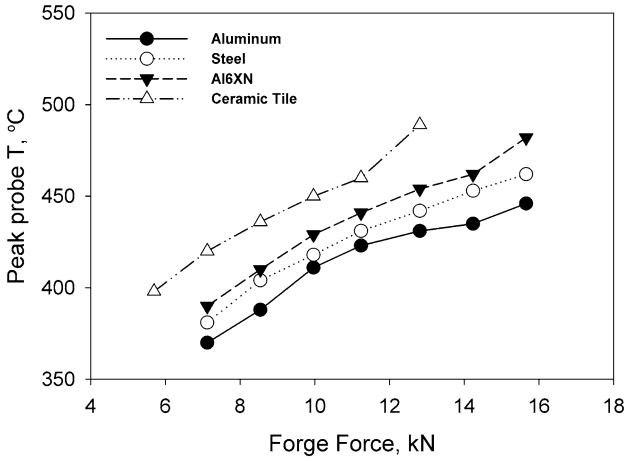

Fig. 4. Measured peak temperature plotted against used forge force from welds made with 4.2-mm-thick AA6056-T6 using aluminum, steel, AL6XN, and ceramic as BP material.

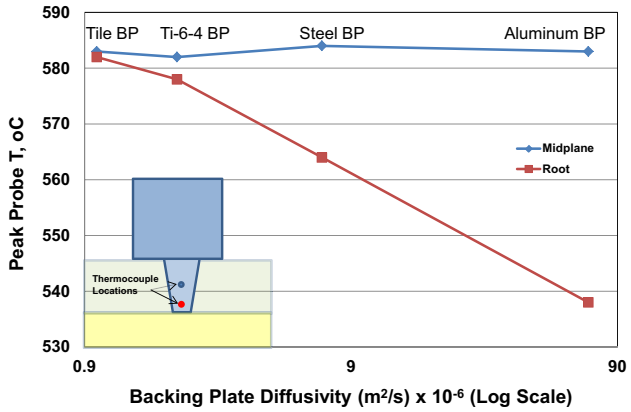

Fig. 5. Measured peak temperature from welds made with 25.4-mm-thick AA6061-T6 using aluminum, steel, Ti-6Al-4V, or ceramic as BP material. The temperature was measured at two indicated locations in the probe.

This increase in the rotation rate/forge force could overheat the crown, causing incipient melting and leading to deteriorated nugget microstructure and undesirable mechanical properties.[29]

Figure 5 shows a plot of measured peak temperature from welds made with four different BPs during FSW of 25.4-mm-thick AA6061-T6. The sketch in the lower left corner of the graph shows the approximate locations of TCs within the tool. With some adjustment of forge force, remarkably similar mid-plane probe temperatures (~584°C) are recorded for all of the BPs. Root temperature, however, varies significantly among the BPs used. Root temperature is the same as the midplane temperature for the ceramic BP case, whereas for the aluminum BP case, the root temperature is 45°C lower. This clearly is the effect of BP thermal properties and shows that the effect of BP diffusivity is highest at the bottom of the workpiece. The effect of this through-thickness temperature variation was clearly observed in weld properties such as hardness and grain size.[30] Because the temperature was homogeneous through the thickness, the weld properties in the nugget, specifically grain size and hardness, were found to be homogenized with the use of a low-thermal-diffusivity BP (such as Ti-6Al-4V or the ceramic) compared with steel or aluminum BPs. However this leads to an unwanted effect; the rate of cooling in the wake of the tool after the weld is produced will be reduced due to insulation at the BP. This in turn may reduce the strength attained after subsequent postweld aging. This is specifically problematic in the HAZ for precipitation-hardening alloys. A composite BP has been shown to circumvent this trade-off. The idea is to use a low-diffusivity central strip about the size of the tip of the tool and a high-diffusivity backing bar for the outer region (see Fig. 6). The low-conductivity strip just under the nugget helps retard the heat escaping from the workpiece, thus enhancing through-thickness homogeneity.

As an aside, the central strip being made, in this case, from tool steel also provides the needed indentation resistance. The high-diffusivity backing bars on either side, on the other hand, will enhance the heat extraction rate, thus decreasing the time at temperature for precipitate coarsening and hence improving the HAZ minimum hardness. The efficacy of the composite BP tested on 25.4-mm-thick AA6061 plates is discussed in a following section.

Nature of Temperature Transients in the Heat-Affected Zone

As described in the foregoing, the temperatures measured at different locations within the tool can provide important information about the temperature in the stir zone, and these temperatures will be representative of the peak temperatures resulting from the welding process. However, for precipitation-hardening alloys, far-field temperatures are equally important, if not more so, in relation to the metallurgical changes that occur in the HAZ. Figure 7 shows a typical weld thermal cycle for IA, UW, and SA conditions for welds made at 3.4 mm/s in AA7050. The data are from TCs placed at the corresponding HAZ minimum hardness locations determined from previous identical weld runs. The peak temperature in the HAZ minimum hardness region is close to 350°C for all cases. This is consistent with the temperatures associated with maximum overaging kinetics of AA7XXX series alloys, which leads to minimum hardness in the HAZ.[1,3,9,26]

The cooling rates calculated from thermal cycles similar to those shown in Fig. 7 but for various welding speeds are shown in Fig. 8. These rates of cooling were calculated over the temperature range of 250°C to 320°C. Clearly, the cooling rates in the HAZ in the UW and SA cases are higher than for the IA case, whereas the difference between the UW and SA cases is very small. This could indicate that for the conditions studied, this subambient condi-

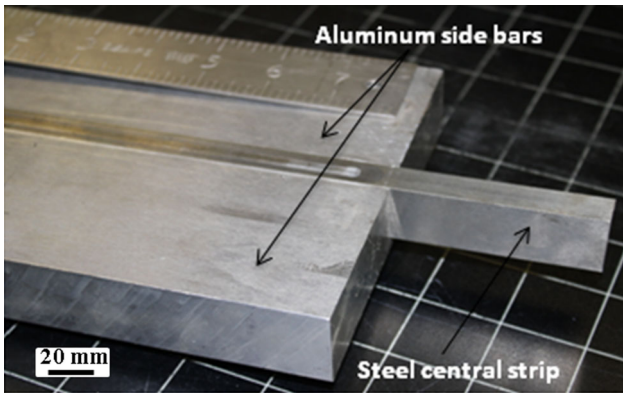

Fig. 6. Example of composite BP.

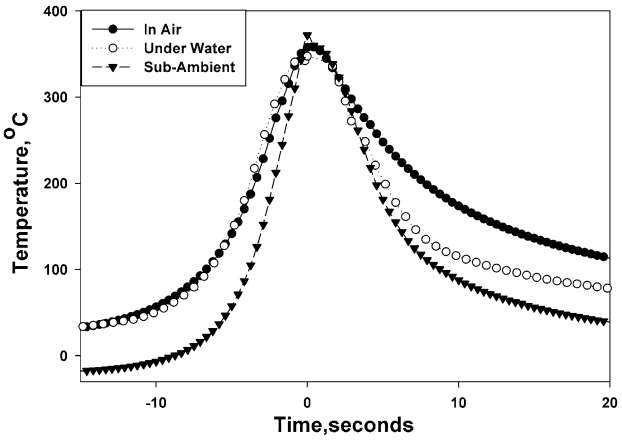

Fig. 7. Temperature history at HAZ minimum hardness location for three different ambient conditions for FSW of 6.35 mm AA7050.

tion does not provide an increased cooling rate over that which is already obtained using room-temperature water. However, it is of interest that similar conditions might be encountered when welding outdoors in harsh conditions such as might be encountered in the arctic. Also, there is hardly any increase in cooling rate beyond the welding speed of 5.1 mm/s. This is indicative of a practical limit to the highest cooling rate achievable for any given welding condition and illustrates the diminishing returns obtained by welding at increasing speed, at least with regard to increased cooling rates. This has been explained using Rosenthal's moving-heat-source equations, wherein temporal length follows a power law with the speed of the heat source.[31]

The cooling rate data obtained from temperatures measured at HAZ locations corresponding to FSWs made in 4.2-mm-thick AA6056 using different BPs with widely varying thermal diffusivity are shown in Fig. 9 on a logarithmic scale. The graph indicates a logarithmically linear relationship between the rate of cooling and the thermal diffusivity of the BP material. Similar instrumentation used on welds of relatively thick (25.4 mm) AA6061 plate shows

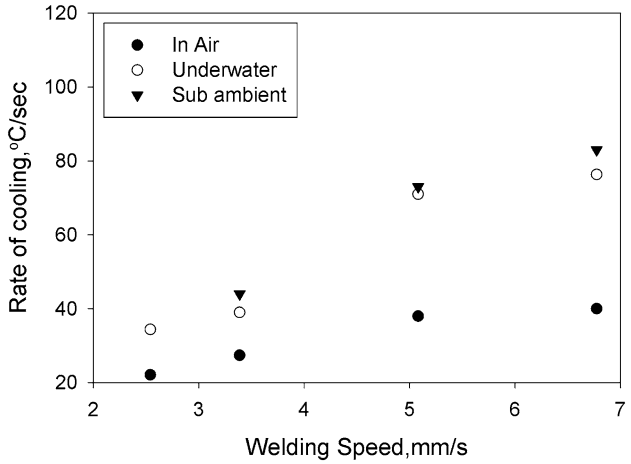

Fig. 8. Rate of cooling over the temperature range of 250°C to 320°C obtained from temperature history measured in the HAZ in FSWs made in 6.35-mm-thick AA7050.

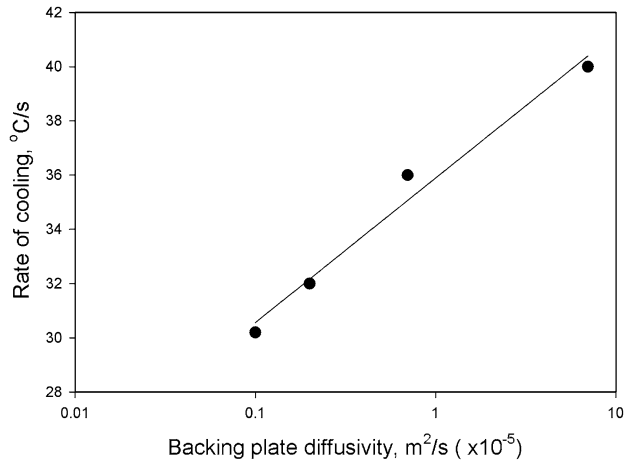

Fig. 9. Rate of cooling over the temperature range of 250°C to 320°C obtained from temperature history measured in the HAZ in FSW of 4.2-mm-thick AA6056 welds.

significantly lower rates of cooling (close to 7°C/s). For the same welding speed and thermal boundary condition, thinner plates (AA7050 and AA6056) discussed previously show much higher rates of cooling (~40°C/s).

Effects of Thermal Boundary Conditions on Weld Properties

Figure 10 shows midplane hardness distributions after postwelding heat treatment (PWHT) to T6 temper for welds made in 6.35-mm-thick AA7050-T7 under three different ambient conditions: IA, UW, and SA. The nugget region exhibits hardness equivalent to a T6 temper and the base metal regions exhibit T7 (slightly overaged) hardness. In the HAZ, substantial overaging has led to a hardness minimum. The shape of the hardness distribution indicates that the nugget region is in a nearly

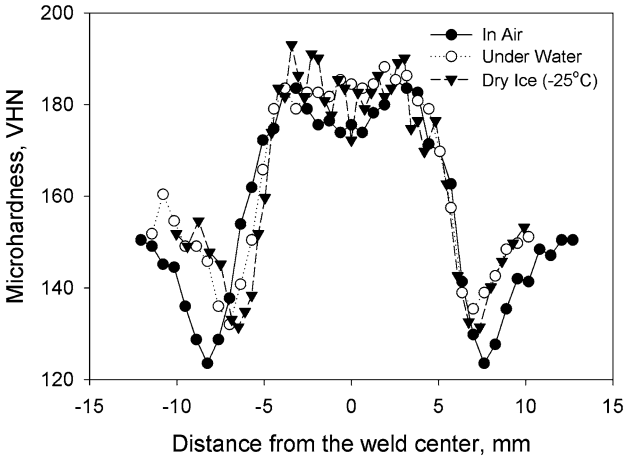

Fig. 10. Representative transverse microhardness distributions across the midplane of friction-stir welded AA7050-T7 PWHT to T6 with three different ambient conditions: in air, underwater, and under a mixture of dry ice and ethylene glycol.

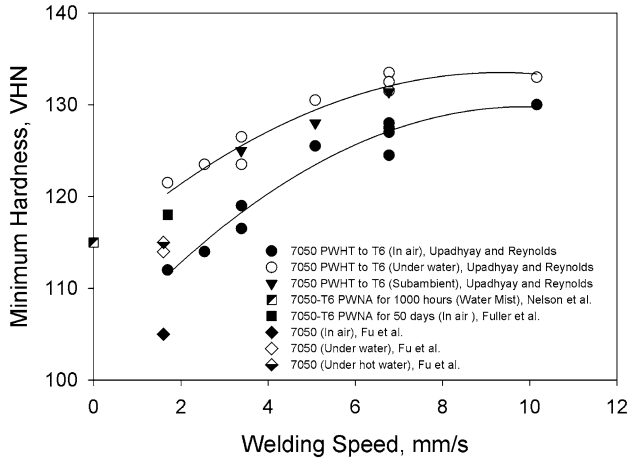

Fig. 11. Average HAZ minimum hardness plotted against the welding speed obtained from different sets of FSW in 7xxx series aluminum alloys using various thermal boundary conditions.

solution-heat-treated condition prior to postweld aging for this set of welding parameters. The hardness minima in the SA and UW welds are not as deep as that observed in the IA weld. Also, the overall width of HAZ is considerably narrower than the IA weld case. Both of these observations can be explained based on the greater cooling rates in the UW and SA cases as observed in Figs. 7 and 8. A higher cooling rate results in shorter exposure time in the temperature range (~350°C) of maximum coarsening kinetics of precipitate phases, thus resulting in a stronger and narrower HAZ.

Figure 11 shows the HAZ minimum hardness from the series of welds made over a wide range of welding and rotational speeds using different boundary conditions. The primary effect illustrated by the graph is that the minimum hardness in the HAZ is strongly dependent on welding speed. Secondarily, active cooling or welding at reduced temperature increases the HAZ minimum hardness. The UW and SA minimum hardness values are consistently higher than that of IA welds made at the same welding speed owing to greater cooling rates at the HAZ. In addition, the difference between minimum hardness values of UW and IA welds is larger at lower welding speeds, thus demonstrating a greater influence of the thermal boundary conditions at lower welding speeds. The graph also shows that the increase in minimum hardness with increasing welding speed is not linear. The increase is rapid at low welding speeds and then slows substantially as welding speed is increased. For the UW welds, almost no increase in minimum hardness is observed above a welding speed of 5.1 mm/s. This observation is consistent with the data in Fig. 9, which indicate that the rate of cooling at the minimum hardness location is not increased substantially by welding at ever-increasing speeds. This is useful from a practical standpoint, suggesting that only a marginal improvement in weld properties can be gained by increasing the welding speed beyond a certain limit.

The effects of BP thermal diffusivity on resulting weld properties are observable in tensile-test data obtained from welds made in 25.4-mm-thick AA6061. Figure 12 shows UTS and percentage elongation in transverse sections for different BP types (conventional steel only, steel/aluminum composite, titanium/aluminum composite, and aluminum only). Clearly, the BP diffusivity has a significant effect on the tensile strength and ductility of the joints. A 25% increase in strength is attained by the use of aluminum as BP in place of conventionally used steel. The elongation of welded joints also significantly increased (from 3% to ~12%) with the use of the aluminum BP. This is likely because the reduced difference between nugget and HAZ minimum hardness leads to lower levels of strain localization during transverse loading of the weld joints. The composite BP, which allowed for homogeneous through-thickness nugget temperature with the use of a low-diffusivity BP underneath the stir zone, also had greater strength and elongation than the monolithic steel BP. This observation is consistent with greater cooling rates measured in the HAZ (see Fig. 9) with the use of a higher-thermal-diffusivity BP.

Figure 13 is a plot of UTS of welds in transverse tension versus welding speed for various welds made in AA7XXX series alloys. Most of the data sets in the figure correspond to previously discussed welds made in 6.35-mm-thick AA7050-T6 PWHT to T6 performed in air, underwater, and in subambient conditions. Additionally, the results from welds made in 7.6-mm-thick AA7136 using a composite BP designed to rapidly cool the workpiece are also reported. The strength values reported in the literature and this work made with different boundary conditions including in air, underwater, and with

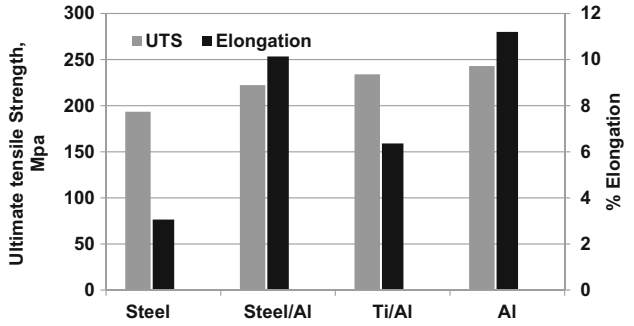

Fig. 12. Transverse tensile strength and percentage elongation of welds made in 25.4-mm-thick AA6061-T6 using different types of BPs.

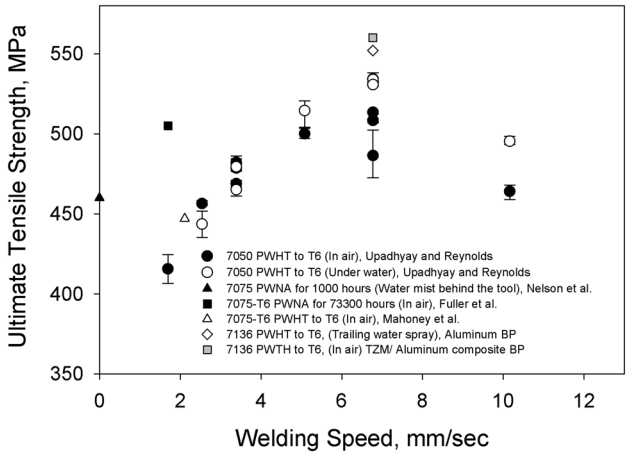

Fig. 13. Transverse tensile strength obtained from welds made in AA7XXX at different thermal conditions.

trailing water mist (see the figure legend for details) are shown in Fig. 13. Note that the data corresponding to Nelson et al.[9] (filled triangle) are plotted on the *Y*-axis because no welding speed was reported in the literature. In general, welds made with enhanced workpiece cooling are consistently stronger than the corresponding in-air cases. There is also a general trend of greater UTS with increasing welding speed up to 6.4 mm/s. The apparent decrease in the strength at the highest welding speed is likely related to overheating of the crown (tool rotation rate = 1000 rpm), resulting in some incipient melting at the nugget. Both the welds made at 10.2 mm/s (UW and IA cases) resulted in failure at the weld nugget during tensile tests rather than the characteristic HAZ failure observed for the rest of the cases. The strengths of welds made in AA7075 reported by Mahoney et al. (shown as an inverted triangle) fall neatly in the strength trend of AA7050. Because of unavailability of welding speed in the case of work by Nelson et al, the value is shown on the *y*-axis.

Of particular interest are the very high strengths achieved in the AA7136 welds (565 MPa, gray square and open diamond). These welds could only be achieved by use of a high-conductivity BP. Standard steel BPs and even steel/aluminum BPs as described previously resulted in overheating for the high weld power levels required for these welds. High strength levels were achieved by welding on monolithic aluminum BPs, but this was often accompanied by the formation of a lap weld between the workpiece and the aluminum BP. Substitution of a titanium-zirconium-molybdenum (TZM) refractory alloy for the tool steel in the composite anvil achieved the twin goals of high BP conductivity and adequate indentation resistance. TZM, along with many other refractory alloys (tungsten or molybdenum based) has a relatively high thermal diffusivity—on par with those of aluminum alloys. The substitution of the TZM strip for the steel strip in the composite BP enabled the production of these very-high-strength welds.

CONCLUSION

Various thermal management methods have been applied during FSW of several types of precipitation-hardening aluminum alloys in a wide range of thicknesses. With all other parameters remaining constant, increased convection from the top surface due to active cooling resulted in reduced nugget temperature, increased torque, and increased cooling rate in the HAZ. The increased cooling rate in the HAZ due to enhanced surface convection resulted in higher HAZ minimum hardness and higher tensile strength of tested transverse weld cross-sections. The temperature measurement at the HAZ and hardness measurements indicated that the time at temperature is only marginally increased by welding beyond a certain welding speed. This is indicative of limited return in property enhancement beyond a certain welding speed. Under the conditions studied, thermal-cycle and hardness measurements show that precooling of the workpiece to −25°C provides a property benefit similar to that obtained from welding under water at ambient temperature, albeit with significantly greater effort. Thermal diffusivity of BP material has a significant effect on the peak temperature achieved at the weld nugget and the cooling rate in the HAZ, which results in a significant variation in weld properties. A wide range of forge force may be used to obtain defect-free welds simply by changing the BP material. The use of a low-thermal-diffusivity BP allows for homogeneous weld temperature in relatively thick sections, whereas a high-thermal-diffusivity BP can enhance cooling rates in the HAZ, resulting in improved HAZ minimum hardness.

ACKNOWLEDGEMENTS

The authors acknowledge the financial support of the Center for Friction Stir Processing, which is a National Science Foundation I/UCRC program (Grant No. EEC-0437341). The authors thank Dr.

Wei Tang and Daniel Wilhelm, Department of Mechanical Engineering, University of South Carolina, Columbia, SC, for their help in preparing the weld joints.

REFERENCES

1. R.S. Mishra and Z.Y. Ma, *Mater. Sci. Eng. R Rep.* 50, 1 (2005).
2. R.S. Mishra, *Scripta Mater.* 58, 325 (2008).
3. P.L. Threadgill, A.J. Leonard, H.R. Shercliff, and P.J. Withers, *Int. Mater. Rev.* 54, 49 (2009).
4. T.W. Eager, *Weld. J.* 74 (1995).
5. K.J. Colligan and R.S. Mishra, *Scripta Mater.* 58, 327 (2008).
6. C.H. Martens, U.S. patent 3282748 (1966).
7. S. Benavides, Y. Li, L.E. Murr, D. Brown, and J.C. McClure, *Scripta Mater.* 41, 809 (1999).
8. C.G. Rhodes, M.W. Mahoney, W.H. Bingel, and M. Calabrese, *Scripta Mater.* 48, 1451 (2003).
9. T.W. Nelson, R.J. Steel, and W.J. Arbegast, *Sci. Technol. Weld. Join.* 8, 283 (2003).
10. J.-Q. Su, T.W. Nelson, R. Mishra, and M. Mahoney, *Acta Mater.* 51, 713 (2003).
11. D.C. Hofmann and K.S. Vecchio, *Mater. Sci. Eng. A* 402, 234 (2005).
12. L. Fratini, G. Buffa, and R. Shivpuri, *Int. J. Adv. Manuf. Technol.* 43, 664 (2008).
13. M. Hosseini and H. Danesh Manesh, *Mater. Des.* 31, 4786 (2010).
14. T. Bloodworth (M.S. thesis, Vanderbilt University, 2009).
15. F. Rui-dong, S. Zeng-qiang, S. Rui-cheng, L. Ying, L. Hui-jie, and L. Lei, *Mater. Des.* 32, 1 (2011).
16. K.J. Colligan, U.S. patent 6516992 (11 February 2003).
17. F. Palm, U.S. patent 6793118 (21 September 2004).
18. S. Kou and G. Cao, U.S. patent 7078647 (18 July 2006).
19. G. Kohn, Y. Greenberg, I. Makover, and A. Munitz, *Weld. J.* 81, 46 (2002).
20. B. M. Tweedy, W. Arbegast, and C. Allen (Paper presented the 2005 TMS Annual Meeting on Friction Stir Welding and Processing III, 2005), pp. 97–104.
21. P.C. Sinclair, W.R. Longhurst, C.D. Cox, D.H. Lammlein, A.M. Strauss, and G.E. Cook, *Mater. Manufact. Proc.* 25, 1283 (2010).
22. A.H. Lotfi and S. Nourouzi, *Int. J. Adv. Manuf. Technol.* 73, 1717 (2014).
23. M.J.C. Rosales, N.G. Alcantara, J. Santos, and R. Zettler, *Mater. Sci. Forum* 636–637, 459 (2010).
24. P. Su, A. Gerlich, T.H. North, and G.J. Bendzsak, *Sci. Technol. Weld. Join.* 11, 163 (2006).
25. D. Bakavos and P.B. Prangnell, *Sci. Technol. Weld. Join.* 14, 443 (2009).
26. Y.S. Sato, M. Urata, and H. Kokawa, *Metall. Mater. Trans. A* 33, 625 (2002).
27. P. Upadhyay and A.P. Reynolds, *Mater. Sci. Eng. A* 527, 1537 (2010).
28. P. Upadhyay and A.P. Reynolds, *Mater. Sci. Eng. A* 558, 394 (2012).
29. M. Moore (M.S. thesis, University of South Carolina, 2007).
30. P. Upadhyay and A. Reynolds, *Metall. Mater. Trans. A* 45, 2091 (2014).
31. D. Rosenthal, *Weld. J.* 20, 220 (1941).